

# A few-emitter solid-state multi-exciton laser

S. Lichtmannecker,<sup>1</sup> M. Florian,<sup>2</sup> T. Reichert,<sup>1</sup> M. Blauth,<sup>1</sup>  
M. Bichler,<sup>1</sup> F. Jahnke,<sup>2</sup> J. J. Finley,<sup>1,\*</sup> C. Gies,<sup>2</sup> and M. Kaniber<sup>1,†</sup>

<sup>1</sup>Walter Schottky Institut and Physik Department,

Technische Universität München, Am Coulombwall 4, 85748 Garching, Germany

<sup>2</sup>Institut für theoretische Physik, Universität Bremen, Otto-Hahn-Allee 1, 28359 Bremen

(Dated: July 3, 2021)

We report a combined experimental and theoretical study of non-conventional lasing from higher multi-exciton states of a few quantum dot-photonic crystal nanocavity. We show that the photon output is fed from saturable quantum emitters rather than a non-saturable background despite being rather insensitive to the spectral position of the mode. Although the exciton transitions of each quantum dot are detuned by up to 160 cavity linewidths, we observe that strong excitation populates a multitude of closely spaced multi-exciton states, which partly overlap spectrally with the mode. The limited number of emitters is confirmed by a complete saturation of the mode intensity at strong pumping, providing sufficient gain to reach stimulated emission, whilst being accompanied by a distinct lasing threshold. Detailed second-order photon-correlation measurements unambiguously identify the transition to lasing for strong pumping and, most remarkably, reveal super-thermal photon bunching with  $g^{(2)}(0) > 2$  below lasing threshold. Based on our microscopic theory, a pump-rate dependent  $\beta$ -factor  $\beta(P)$  is needed to describe the nanolaser and account for the interplay of multi-exciton transitions in the few-emitter gain medium. Moreover, we theoretically predict that the super-thermal bunching is related to dipole-anticorrelated multi-exciton recombination channels via sub- and super-radiant coupling below and above lasing threshold, respectively. Our results provide new insights into the microscopic light-matter-coupling of spatially separated emitters coupled to a common cavity mode and, thus, provides a complete understanding of stimulated emission in nanolasers with discrete emitters.

Self-assembled semiconductor quantum dots (QDs) exhibit richer discrete energy level structures compared to atoms, due to their mesoscopic size, shape and dielectric surroundings [1]. When embedded within nanostructured photonic cavities, QDs allow for the investigation of cavity quantum electrodynamics phenomena in the solid state and provide strong potential for photon mediated quantum information technologies in a uniquely scalable architecture [2]. Photonic crystal (PhC) [3] nanostructures in particular provide strong optical confinement in high quality (Q) factor and small mode volume ( $V_{\text{mode}}$ ) cavities [4], making them suitable to explore the miniaturization limit of lasing where the gain medium consists only of a few solid-state quantum emitters within a single mode cavity. Recent experiments performed on PhC cavities have demonstrated stimulated emission and lasing [5–8]. Moreover, the rich multi-exciton structure provided by the QDs has been shown to play a significant role in far-off resonant cavity feeding and photon bunching from PhC cavities [9, 10]. Similar results of photon bunching and a clear transition to coherent emission and lasing operation were demonstrated in micropillar cavities subject to optical excitation or electrical injection [11, 12].

In this letter, we observe a transition from spontaneous to non-conventional lasing from an L3 PhC nanocavity loaded with a few ( $N \sim 4$ ) spectrally detuned QDs. The intensity of the cavity mode emission as a function of the excitation level exhibits a weak threshold, indicative of a transition to lasing for a level very close to the saturation

power density of nearby QDs  $P_{\text{sat}}^{\text{QD}} \sim 0.14 \pm 0.1 \text{ kW/cm}^2$ . Moreover, the input-output characteristic of the device shows a complete saturation for excitation power densities of  $P_{\text{sat}}^{\text{cav}} > 4.7 \pm 0.4 \text{ kW/cm}^2$ , demonstrating that the cavity mode emission is fed from saturable emission from a few QDs, rather than a broadband non-saturable background [7]. The transition to lasing is identified via second-order photon-correlation spectroscopy performed on the detuned cavity-mode emission that shows super-thermal photon bunching at zero time delay with  $g^{(2)}(0) > 2$  at low power densities, and an unambiguous transition to coherent light emission with  $g^{(2)}(0) = 1$  at elevated excitation. Remarkably, the experimental results are shown to be insensitive to the mean detuning between the QDs and the cavity. Insights into the underlying physical mechanisms responsible for lasing are gained from theoretical simulations that take into account multi-exciton states of four QDs spatially located in the cavity region, and their non-perturbative interaction with the photons in the laser mode. On the basis of the theoretical model, we introduce a pump-rate dependent  $\beta$ -factor  $\beta(P)$  that characterizes the spontaneous emission coupling into the cavity mode. We show that the interplay of multi-exciton transitions in the few-emitter gain medium gives rise to a strong pump-density dependence of  $\beta(P)$ . As such, we show that the system is not well described in terms of the constant  $\beta$ -factor that is used in conventional laser theories. Radiative coupling between spatially separated emitters mutually coupled to the strongly confined cavity field has

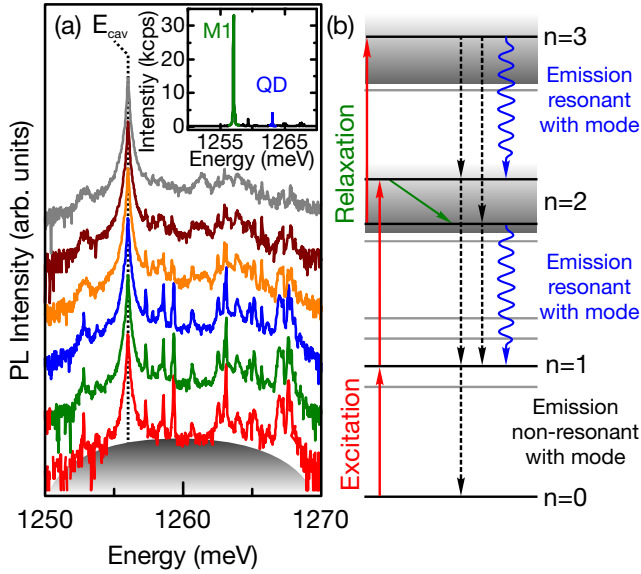


Figure 1. (a) Emission spectra from the cavity increasing cw excitation power density from  $0.14 \text{ kW/cm}^2$  to  $5.9 \text{ kW/cm}^2$ . The spectra are plotted on a logarithmic scale with offset to each other for clarity. The cavity mode is labeled  $E_{\text{cav}}$ . The inset shows a linear spectrum of the system for an excitation power density of  $P_{\text{sat}}^{\text{QD}}$ . (b) Schematic level schema of the manifolds of multi-excitonic emission channels with  $n = 0 \dots 3$  excitations. The arrows indicate the physical excitation, relaxation, and recombination processes that are included in the theoretical modeling, as explained in the text.

recently been predicted to lead to sub- and superradiant effects in nanolasers [13, 14]. From our theoretical analysis, the super-thermal bunching is identified to arise from dipole-anticorrelated multi-excitonic emission channels that emit subradiant light below threshold. The transition from subradiant emission to superradiant lasing is also reflected in the pump-dependent factor  $\beta(P)$ . Our work provides new insights to the lasing mechanism, spontaneous emission coupling factor and radiative QD-QD coupling in few-dot nanocavity lasers.

To characterize our system, we show in figure 1 (a)  $\mu$ -PL spectra on a stacked logarithmic scale recorded with cavity mode resonant excitation via the third order cavity mode [15, 16] using an excitation power density increasing from  $0.14 \text{ kW/cm}^2$  (bottom spectrum) to  $5.9 \text{ kW/cm}^2$  (top spectrum). The spectra show the cavity mode emission at  $E_{\text{cav}} = 1257.1 \text{ meV}$  and the emission of a few ( $N \sim 4$ ) QDs located in the PhC nanocavity. The emission of these QDs evolves into a broadband emission attributed to multi-exciton transitions for elevated excitation intensities, as highlighted by the gray shaded region [9]. The inset shows a spectrum in a linear representation for an excitation power density of  $0.14 \text{ kW/cm}^2$  close to the saturation power density  $P_{\text{sat}}^{\text{QD}}$  of the single QD emitting at  $E_{\text{QD}} = 1263.1 \text{ meV}$ , highlighted in blue. Fitting the fundamental cavity mode M1 (highlighted in

green) with a Lorentzian line yields a full width at half maximum of  $\Delta E = 104 \pm 2 \text{ meV}$  corresponding to a moderate mode  $Q = E_{\text{cav}}/\Delta E \approx 12000$ . Measuring the auto-correlation function of the QD emission at  $E_{\text{QD}}$  reveals the single-photon character of the emission, and the cross correlation measurement of the QD and the M1 cavity mode (shown in the Supplementary Material) proves non-resonant coupling through antibunched emission despite the large initial energy detuning of  $\Delta_{\text{QD-M1}} = 6 \text{ meV}$  [17–21].

On the basis of this characterization, we consider a theoretical model that accounts for the key elements of the experiment, namely the interplay of multi-excitonic emission channels from several different QD emitters, and their light-matter interaction with photons in the cavity mode. We assume that each QD possesses a multitude of many-particle states represented by different number  $n$  of excitations in the form of e-h-pairs and their distribution over the available many-particle states [10]. For the  $n = 1$  to  $n = 0$  transition only well-separated emission lines exist, whereas for  $n = 2$  to  $n = 1$  and  $n = 3$  to  $n = 2$  a large number of possible transitions result in a broad range of closely spaced lines resembling a quasi-continuous spectrum [9], as illustrated in figure 1 (b). To model the emission characteristics, we solve the von Neumann-Lindblad equation for the density matrix of the coupled carrier-photon system with non-perturbative Jaynes-Cummings interaction. Due to the large state space, calculations can only be performed for a subset of the QD many-particle configurations. For each QD, we choose two multi-exciton configurations whose recombination is resonant with the cavity mode, whereas the ground state exciton transition is strongly detuned. This allows us to study the interplay of QD many-particle states and the resulting coupling to the cavity mode within a wide spectral window. Excitation and relaxation processes indicated in figure 1(b) are described by Lindblad terms. Details of the microscopic model are found in the supplementary material.

In figure 2 (a) we present the integrated (green symbols) and calculated (red line) PL intensity of the cavity as a function of excitation power density, as well as the QD emission (blue symbols). Fitting a power law  $I = A \cdot P^m$  to the intensity  $I$  of the QD reveals a linear behaviour with an exponent  $m^{\text{QD}} = 0.91 \pm 0.03$  as shown by the black line, indicating single excitonic character of the emission line [22]. Moreover, the QD emission saturates at an excitation power density of  $P_{\text{sat}}^{\text{QD}} = 0.14 \pm 0.1 \text{ kW/cm}^2$  as highlighted by the dotted black line in figure 2 (a). For the cavity mode emission we observe a similar behavior for excitation power densities  $P < P_{\text{sat}}^{\text{QD}}$ , reflected by an exponent  $m_1^{\text{cav}} = 1.06 \pm 0.02$ . For excitation power densities  $P_{\text{sat}}^{\text{QD}} < P < P_{\text{sat}}^{\text{cav}}$  we observe a slight superlinear increase, giving rise to an exponent of  $m_2^{\text{cav}} = 1.22 \pm 0.07$ , highlighted in orange in figure 2 (a). The increase in the exponent of the cav-

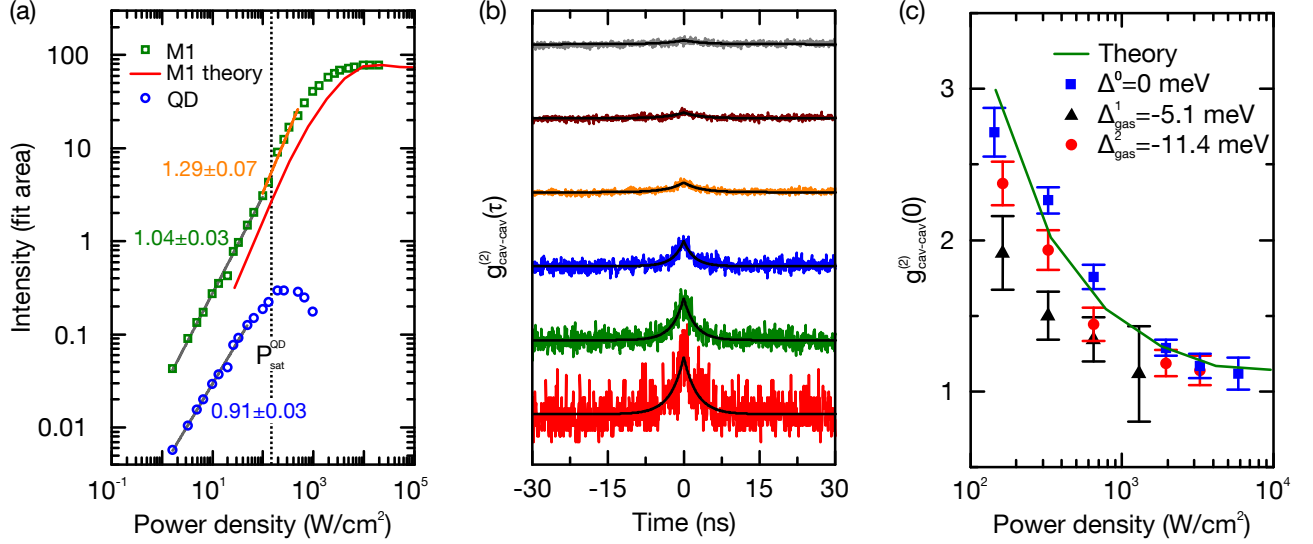


Figure 2. (a) Integrated intensity of the cavity mode (green) and the QD (blue) as a function of excitation power density. Black solid lines represent power-law fits to the emission data. The solid red line depicts the intensity of the cavity mode emission calculated from theory. To connect the theoretical pump rate with the experimental power density, the red curve has been shifted along the power axis to ensure that the calculated exciton saturation coincides with  $P_{\text{sat}}^{\text{QD}}$ . (b) Auto-correlation measurements of the cavity mode for the accordingly color coded spectra presented in figure 1 (a) ( $\Delta^0$  in figure 2 (c)). Solid black lines are fits to the data. (c) Second order correlation  $g_{\text{cav-cav}}^{(2)}(0)$  as function of the excitation power density. The colors represent three different cavity mode energies, blue  $\Delta^0 = 0$  meV  $\equiv E_{\text{cav}}$ , black  $\Delta_{\text{gas}}^1 = -5.1$  meV and red  $\Delta_{\text{gas}}^2 = -11.4$  meV. The solid green line is the numerical result  $g^{(2)}(0)$  from theory.

ity intensity power dependence appears simultaneously with the saturation of the QD, when multi-exciton states become increasingly populated with significant probability. For even higher excitation power densities  $P > P_{\text{sat}}^{\text{cav}} = 4.7 \pm 0.4$  kW/cm² a complete saturation of the mode emission is observed. This finding unambiguously confirms the absence of non-saturable background contributions and reflects the limited gain the few QDs are able to provide. The calculated input-output-characteristic (red curve) reproduces the main features that are seen in the experimental data, namely a nearly thresholdless increase and full saturation of the output. The slight kink in the input-output characteristic of the mode emission in combination with the observed saturation behavior gives rise to a moderate s-shape curve typical for nanolasers [23] with ultra-low thresholds [6, 7]. Procedures from rate equations for conventional lasers might suggest to estimate a  $\beta$ -factor from this kink, see e.g. Ref. [7, 20], however, we will demonstrate that the underlying mechanism of multi-exciton lasing requires an entirely different approach, as we explain below in the context of figure 3.

It is well recognized that photon autocorrelation measurements provide a clear indication for lasing in the absence of a visible threshold in the input-output characteristics. In order to support our previous hypothesis of a low-threshold, few-QD nanolaser, we present detailed investigations of  $g_{\text{cav-cav}}^{(2)}(\tau)$  for the cavity mode emission. For each of the color-coded excitation power densities

shown in figure 1 (a) we performed second-order photon correlation measurements of the cavity mode  $g_{\text{cav-cav}}^{(2)}(\tau)$  which are presented in figure 2 (b). Fitting the data with  $g^{(2)}(\tau) = 1 + A \cdot \exp(-2|\tau|/t_0)$  (shown by the black lines) [24] enables us to extract the zero-time-delay values of  $g_{\text{cav-cav}}^{(2)}(0)$  shown by the blue symbols in figure 2 (c). Upon increasing the excitation level from 0.14 kW/cm² to 5.9 kW/cm² we demonstrate a clear transition from the spontaneous-emission regime with  $g_{\text{cav-cav}}^{(2)}(0) \gg 1$  to lasing with  $g_{\text{cav-cav}}^{(2)}(0) = 1$  [11]. The photon auto-correlation function is also readily available within the density-matrix formalism [25], and the theoretical model predicts the same qualitative and quantitative behavior, as shown by the green line in figure 2 (c).

Interestingly, in the low-excitation regime super-thermal values up to  $g^{(2)}(0) = 2.71 \pm 0.16$  are observed in figure 2 (c) both in theory and experiment. They exceed the values reported in previous experimental studies [7, 9] by a factor of 2, and even the theoretical limit of 2 for thermal light. The enhanced probability of two- and multiple-photon emission events reflected by  $g^{(2)}(0) > 2$  is attributed to the presence of competing resonant emission channels for each QD emitter, allowing for the simultaneous emission of photons into the mode. Moreover, in the numerical calculation we observe the presence of strong radiative coupling effects (see the discussion of figure 3). Such effects have been predicted to leave a super-thermal finger print in cw-excited nanolasers at

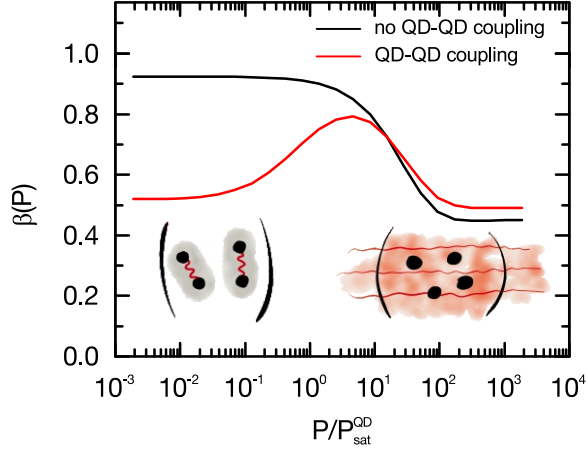


Figure 3. (Red curve) pump-rate dependent  $\beta$ -factor obtained from the theoretical model with parameters applicable to experimentally studied system. (Black curve) calculation suppressing radiative coupling effects between emitters that are responsible for sub- and superradiant effects. Comparing both curves reveals that radiative coupling effects lead to a strong inhibition of spontaneous emission at low excitation (subradiance) and a slight enhancement of spontaneous emission above the laser threshold (superradiance).

low-excitation powers [13, 14, 26]. We interpret the experimental observation of the super-thermal bunching as proof for a new regime of spontaneous emission with radiatively enhanced correlations between distant emitters inside the nanocavity.

To shed more light on the efficiency of non-resonant coupling, we have studied the influence of cavity emitter detuning  $\Delta$  on the cavity-mode correlation function  $g_{\text{cav-cav}}^{(2)}(\tau)$  by red-shifting the cavity mode energy by locally freezing inert nitrogen into the PhC [16, 27]. Figure 2 (c) shows the experimentally determined values of  $g_{\text{cav-cav}}^{(2)}(0)$  as a function of excitation power density for three different cases with dot-cavity detunings,  $\Delta^0 = 0$  meV (blue squares),  $\Delta_{\text{gas}}^1 = -5.1$  meV (black triangles) and  $\Delta_{\text{gas}}^2 = -11.4$  meV (red circles). Similar behavior of  $g_{\text{cav-cav}}^{(2)}(0)$  is observed for all detunings, namely a clear transition from spontaneous emission to lasing. Coherent emission is clearly reached at  $P = 10^3$  W/cm<sup>2</sup> for all cases before the onset of cavity mode saturation. Furthermore, we observe that the efficiency of the non-resonant coupling makes nanolaser operation rather robust for total spectral cavity-emitter detunings up to  $\Delta \sim 17$  meV. Thus, the absolute energies of QD-transitions and cavity mode are of limited importance for the operation of the nanolaser. This finding further motivates the simplification of considering only resonant multi-excitation transitions in the microscopic modeling.

We now turn to the characterization of spontaneous emission coupling in the presence of multi-exciton lasing. The  $\beta$ -factor quantifies the fraction of the total spon-

aneous emission that is directed into the laser mode. From a rate equation model it is found that  $\beta$  is solely determined by the relation of the rates associated with emission into the laser mode  $\gamma$  and into non-lasing modes or other loss channels  $\gamma_{\text{nl}}$ , i.e.,  $\beta = \gamma/(\gamma + \gamma_{\text{nl}})$ . In the rate equations, the rates are understood to be ensemble averages of two-level systems. However, if the gain material consists of only few solid-state emitters, multi-exciton transitions from different emitters may tune in and out of resonance with the cavity mode as pumping is varied. Thus, the coupling efficiency to the cavity mode varies for each of these emission channels, which must be accounted for when formulating the  $\beta$ -factor for few-QD nanolasers. To obtain a quantity that reflects this behavior, we calculate for each pump rate the averaged spontaneous emission rate of the QD ensemble from the spontaneous emission contribution  $\Gamma$  to the photon-assisted polarization [13], which is given by

$$\Gamma = \sum_{i,j} \left[ \sum_{\alpha=1}^{N_{\text{QD}}} R_i \left\langle (D_{\alpha,i}^l)^\dagger D_{\alpha,j}^l \right\rangle \delta_{i,j} + \sum_{\alpha \neq \beta}^{N_{\text{QD}}} R_i \left\langle D_{\alpha,i}^l (D_{\beta,j}^l)^\dagger \right\rangle \right]. \quad (1)$$

Here, the operator  $D_{\alpha,i}^l$  describes an allowed (bright) dipole transition between multi-exciton states, e.g. from exciton to ground state, in QD  $\alpha$ , with the initial state  $|i_\alpha\rangle$ , and the corresponding recombination rate  $R_i$ . The quantum-mechanical average is taken with respect to the steady-state density operator. The first sum in Eq. (1) includes all bright transitions, while the sums in the brackets address the QD emitters in the gain medium. We distinguish two contributions: The first term in the brackets is the sum of the spontaneous emission contributions from all emitters *independently*, while the second sum is the contribution of *dipole-correlated transitions in different emitters*, which arises due to radiative coupling. In figure 3 we show the pump-rate dependent factor  $\beta(P)$  calculated from this rate  $\Gamma$  including (red curve) and excluding (black curve) radiative emitter coupling, and under consideration of the loss-rates as given by the Lindblad terms. For further details of the theoretical description, we refer to the Supplementary Material. Without radiative coupling effects (black curve), a transition is seen from  $\beta(P) > 90\%$  to  $\beta(P) \approx 50\%$  as the system switches between multi-excitonic emission channels from different manifolds, as schematically depicted in figure 1(b). These limiting values at low and high excitation reflect the conventional constant  $\beta$ -factor associated with these transitions. This behavior is drastically changed due to radiative coupling effects (red curve), which cause a strong inhibition of the spontaneous emission rate below threshold, resulting in  $\beta(P) = 50\%$  instead of 90% at low excitation. Spontaneous emission



inhibition has been identified previously as subradiance due to an anti-correlation of dipoles in different emitters [13]. In Eq. 1 it results from a negative contribution from the second term. At excitation powers  $\gtrsim 20P_{\text{sat}}^{QD}$ , the sign changes and spontaneous emission is enhanced due to *superradiant* coupling between emitters.

While we can directly quantify the effect of sub- and superradiant inter-emitter coupling in the spontaneous emission rate, it is not straightforward to switch off inter-emitter coupling in the numerical results shown in figure. 2, and even less so in the experiment. However, the comparison in figure 3, together with the super-thermal bunching observed at weak excitation as shown in figure 2(c), provides a strong account for the presence of radiative coupling in the QD nanocavity system that is supported by predictions made in Ref. [13].

Finally, we point out that a kink in the input-output characteristics can be misinterpreted in terms of a constant  $\beta$ -factor, but may in fact result from transitions between multi-exciton states of various emitters tuning in and out of resonance at various excitation powers.

In summary, we presented new insight into the extraordinary operational regime of a few ( $\sim 4$ ) solid-state emitter PhC nanolaser. We have observed super-thermal bunching of the emission and explained it on the basis of a microscopic theory to arise from the simultaneous presence of different resonant emission channels and their radiative coupling. We have further demonstrated that a conventional single-valued  $\beta$ -factor cannot characterize the interplay of multi-exciton lasing in few-emitter QD lasers. The newly introduced factor  $\beta(P)$  is pump-rate dependent and strongly determined by radiative coupling effects. In combination with the super-thermal bunching, it gives strong account for the presence of radiative coupling effects in the form of sub- and superradiance in the nanolaser system. At elevated excitation powers, lasing is demonstrated, while full saturation of the emissions at the highest excitation powers proves that only a few saturable multi-exciton states contribute to the excitation, and that continuum states from the wetting layer are not necessary for lasing operation in our device.

*Acknowledgements:* We thank F.P. Laussy and E. del Valle for highly fruitful discussions and gratefully acknowledge financial support from the DFG via SFB 631, JA 619/10-3, JA 619/13-1 and GI 1121/1-1, the German Excellence Initiative via NIM, as well as from the BMBF via QuaHL-Rep and Q.com.

---

\* [jonathan.finley@wsi.tum.de](mailto:jonathan.finley@wsi.tum.de)

† [michael.kaniber@wsi.tum.de](mailto:michael.kaniber@wsi.tum.de)

[1] D. Bimberg, M. Grundmann, and N. N. Ledentsov, *Quantum dot heterostructures* (John Wiley & Sons, 1999).

- [2] J. L. O'Brien, A. Furusawa, and J. Vučković, *Nature Photonics* **3**, 687 (2009).
- [3] J. D. Joannopoulos, P. R. Villeneuve, and S. Fan, *Nature* **386**, 143 (1997).
- [4] S. Noda, M. Fujita, and T. Asano, *Nature photonics* **1**, 449 (2007).
- [5] J. Hendrickson, B. Richards, J. Sweet, S. Mosor, C. Christenson, D. Lam, G. Khitrova, H. Gibbs, T. Yoshie, A. Scherer, et al., *Physical Review B* **72**, 193303 (2005).
- [6] S. Reitzenstein, A. Bazhenov, A. Gorbunov, C. Hofmann, S. Münch, A. Löffler, M. Kamp, J. Reithmaier, V. Kulakovskii, and A. Forchel, *Applied physics letters* **89**, 1107 (2006).
- [7] S. Strauf, K. Hennessy, M. Rakher, Y.-S. Choi, A. Badolato, L. Andreani, E. Hu, P. Petroff, and D. Bouwmeester, *Physical review letters* **96**, 127404 (2006).
- [8] H. Altug, D. Englund, and J. Vučković, *Nature Physics* **2**, 484 (2006).
- [9] M. Winger, T. Volz, G. Tarel, S. Portolan, A. Badolato, K. J. Hennessy, E. L. Hu, A. Beveratos, J. Finley, V. Savona, et al., *Physical review letters* **103**, 207403 (2009).
- [10] A. Laucht, M. Kaniber, A. Mohtashami, N. Hauke, M. Bichler, and J. Finley, *Physical Review B* **81**, 241302 (2010).
- [11] S. Ulrich, C. Gies, S. Ates, J. Wiersig, S. Reitzenstein, C. Hofmann, A. Löffler, A. Forchel, F. Jahnke, and P. Michler, *Physical review letters* **98**, 043906 (2007).
- [12] C. Schneider, A. Rahimi-Iman, N. Y. Kim, J. Fischer, I. G. Savenko, M. Amthor, M. Lerner, A. Wolf, L. Worschech, V. D. Kulakovskii, et al., *Nature* **497**, 348 (2013).
- [13] H. Leymann, A. Foerster, F. Jahnke, J. Wiersig, and C. Gies, *Physical Review Applied* **4**, 044018 (2015).
- [14] E. Mascarenhas, D. Gerace, M. F. Santos, and A. Auffèves, *Physical Review A* **88**, 063825 (2013).
- [15] A. Chalcraft, S. Lam, D. O'Brien, T. Krauss, M. Sahin, D. Szymanski, D. Sanvitto, R. Oulton, M. Skolnick, A. Fox, et al., *Applied Physics Letters* **90**, 241117 (2007).
- [16] M. Kaniber, A. Laucht, A. Neumann, M. Bichler, M. Amann, and J. Finley, *Journal of Physics: Condensed Matter* **20**, 454209 (2008).
- [17] K. Hennessy, A. Badolato, M. Winger, D. Gerace, M. Atatüre, S. Gulde, S. Fält, E. L. Hu, and A. Imamoglu, *Nature* **445**, 896 (2007).
- [18] D. Press, S. Götzinger, S. Reitzenstein, C. Hofmann, A. Löffler, M. Kamp, A. Forchel, and Y. Yamamoto, *Physical Review Letters* **98**, 117402 (2007).
- [19] M. Kaniber, A. Laucht, A. Neumann, J. Villas-Bôas, M. Bichler, M.-C. Amann, and J. Finley, *Physical Review B* **77**, 161303 (2008).
- [20] P. Michler, A. Kiraz, C. Becher, W. Schoenfeld, P. Petroff, L. Zhang, E. Hu, and A. Imamoglu, *Science* **290**, 2282 (2000).
- [21] C. Santori, M. Pelton, G. Solomon, Y. Dale, and Y. Yamamoto, *Physical Review Letters* **86**, 1502 (2001).
- [22] J. Finley, A. Ashmore, A. Lemaître, D. Mowbray, M. Skolnick, I. Itskevich, P. Maksym, M. Hopkinson, and T. Krauss, *Physical Review B* **63**, 073307 (2001).
- [23] G. Björk, A. Karlsson, and Y. Yamamoto, *Applied physics letters* **60**, 304 (1992).

- [24] R. Loudon, *The quantum theory of light* (Oxford university press, 2000).
- [25] M. Florian, P. Gartner, C. Gies, and F. Jahnke, New Journal of Physics **15**, 035019 (2013).
- [26] A. Auffeves, D. Gerace, S. Portolan, A. Drezet, and M. F. Santos, New Journal of Physics **13**, 093020 (2011).
- [27] S. Mosor, J. Hendrickson, B. Richards, J. Sweet, G. Khitrova, H. Gibbs, T. Yoshie, A. Scherer, O. Shchekin, and D. Deppe, Applied Physics Letters **87**, 141105 (2005).

# Supplementary Material: A few-emitter solid-state multi-exciton laser

S. Lichtmannecker,<sup>1</sup> M. Florian,<sup>2</sup> T. Reichert,<sup>1</sup> M. Blauth,<sup>1</sup>  
M. Bichler,<sup>1</sup> F. Jahnke,<sup>2</sup> J. J. Finley,<sup>1,\*</sup> C. Gies,<sup>2</sup> and M. Kaniber<sup>1,†</sup>

<sup>1</sup>Walter Schottky Institut and Physik Department,

Technische Universität München, Am Coulombwall 4, 85748 Garching, Germany

<sup>2</sup>Institut für theoretische Physik, Universität Bremen, Otto-Hahn-Allee 1, 28359 Bremen

(Dated: July 3, 2021)

## FABRICATION AND EXPERIMENTAL DETAILS

The sample investigated was grown using molecular beam epitaxy on a 350  $\mu\text{m}$  thick [100] GaAs wafer. A 300 nm GaAs buffer layer was grown, followed by an 800 nm thick sacrificial layer of  $\text{Al}_{0.8}\text{Ga}_{0.2}\text{As}$  and an 150 nm thick nominally undoped GaAs slab that contained a single layer of nominally  $\text{In}_{0.5}\text{Ga}_{0.5}\text{As}$  QDs at its midpoint. The growth conditions used for the QD layer yielded an areal density  $\rho_D \sim 20 \mu\text{m}^{-2}$ , emitting over the spectral range of 1270 – 1400 meV. After growth, a hexagonal lattice of air holes was defined by electron beam lithography with a lattice constant of  $a = 270 \text{ nm}$  in a ZEP 520-A soft mask and deeply etched using a  $\text{SiCl}_4$  based inductively coupled plasma to form a 2D PhC [1]. We incorporated an optimized L3 cavity design [2, 3], giving rise to cavities with  $V_{\text{mode}} \sim 0.92(\lambda/n)^3$  and  $Q = 8000 - 15000$ . In a final process step the AlGaAs layer was selectively removed with hydrofluoric acid to establish a free standing membrane.

For optical studies the sample was mounted in a liquid He flow-cryostat and cooled to lattice temperatures of  $T = 12 \text{ K}$ . Excitation of the sample was achieved via a  $100\times$  high numerical aperture  $NA = 0.5$  confocal microscope objective that enables to focus light to a diffraction limit spot with  $1/e^2$ -size of 960 nm. The optical response from the system was collected via the same microscope objective and directly guided to a single imaging monochromator and detected with a liquid nitrogen cooled CCD camera. For measurements of the second order photon correlation function  $g^{(2)}(\tau)$ , the monochromator was used as a tunable bandpass filter with a bandwidth of 270  $\mu\text{eV}$ . The spectrally filtered signal was coupled into a fiber-beamsplitter and guided to two separate avalanche photo diodes which provide single photon sensitivity and act as a Hanbury Brown and Twiss setup [4]. The avalanche photo diodes exhibit a temporal resolution of 350 ps. The detection events were time correlated using a Pico Quant TimeHarp time tagging module. For mode resonant excitation [5, 6] we used a continuous wave single frequency laser with a bandwidth of 100 kHz and a tuning range between 1259 meV and 1369 meV.

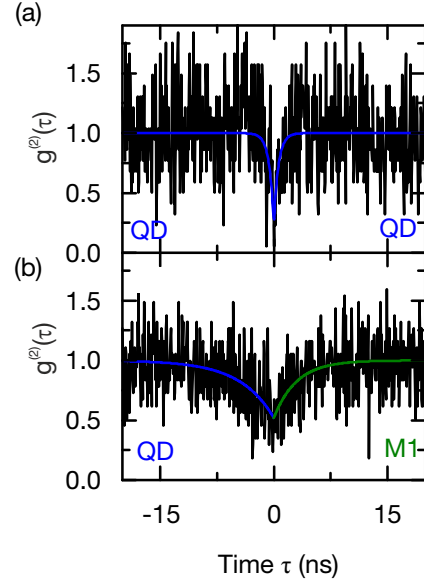


Figure SM 1. (a) Second-order autocorrelation measurement of QD emitting at  $E_{\text{QD}} = 1263.1 \text{ meV}$  as shown in Figure 1a (main manuscript). (b) Second-order cross-correlation measurement between QD emitting at  $E_{\text{QD}} = 1263.1 \text{ meV}$  and the cavity mode M1 emitting at  $E_{\text{cav}} = 1257.1 \text{ meV}$  as shown in Figure 1a (main manuscript).

## AUTO- AND CROSS-CORRELATION SPECTROSCOPY

To gain more insight into the coupling between the spectrally detuned QD and the cavity mode we performed measurements of the photon statistics of the emitted light. First we measured the second order photon correlation function  $g^{(2)}(\tau)$  of the QD emitting at 1263.1 meV with an excitation power density close to saturation ( $\sim 0.14 \text{ kW/cm}^2$ ) as shown in figure SM1 (a). For zero time delay  $\tau = 0 \text{ ns}$  we observe a reduced number of correlation counts, giving rise to a value of  $g_{X-X}^{(2)}(0) = 0.25 \pm 0.16$ , demonstrating the non-classical character of the studied quantum light and indicating that the signal stems pre-dominantly from a single quantum emitter [7, 8]. As we have proven the single photon characteristics of the emission we investigated the coupling of the QD to the fundamental cavity mode M1 by performing cross-correlation measurements between

them. The measurement of the cross-correlation function  $g_{X-cav}^{(2)}(\tau)$  is presented in figure SM1 (b) for the same excitation power density of  $\sim 0.14 \text{ kW/cm}^2$ . As for the autocorrelation measurement of the QD, the measurement between QD and cavity mode yields a strong suppression of correlations for zero time delays with a  $g_{X-cav}^{(2)}(0) = 0.52 \pm 0.07$ . This antibunching unambiguously proves that the investigated QD is efficiently coupled to the cavity mode, since we would expect an uncorrelated constant statistic  $g_{X-cav}^{(2)}(\tau) = 1$  for an uncoupled QD and cavity [9–11]. This non-resonant cavity mode feeding has been shown to be due to a number of mechanisms including coupling to acoustic phonons [12] and higher excited QD transitions [13]. The slightly increased value of  $g_{X-cav}^{(2)}(0) = 0.52 \pm 0.07$  is attributed to additional sources of cavity feeding, most probably due to other spectrally detuned QD transitions. The different lifetimes  $\tau_{auto}^{QD} = 0.61 \pm 0.19 \text{ ns}$  and  $\tau_{cross}^{QD} = 3.0 \pm 0.65 \text{ ns}$ , extracted from the auto-correlation and cross-correlation measurement in figure SM1 (a) and (b), respectively, are due to different spectral cavity mode-QD detunings  $\Delta_{auto}^{cav-QD} = 6.1 \text{ meV}$  and  $\Delta_{cross}^{cav-QD} = 7.7 \text{ meV}$ , respectively. We conclude that we are investigating a state of the art nano-cavity doped with few single photon emitters that are efficiently non-resonantly coupled to the cavity mode via their multi-exciton states. Complete saturations of the cavity mode emission proves that the cavity mode is only pumped by a few QD states.

## THEORETICAL METHODS

In this section we discuss the theoretical model underlying the results shown in figure 2 (main manuscript) and provide details about the calculation of the  $\beta(P)$ -factor presented in figure 3 (main manuscript). For the theoretical description we consider an ensemble of  $N_{QD} = 4$  self-assembled QDs coupled to a single high-quality mode of the PhC cavity. Each QD  $\alpha$  possesses a multitude of many-particle states  $|i_\alpha\rangle$ , represented by different excitation manifolds  $n$ , where  $n$  stands for the total excitation number of e-h-pairs in the QD (compare figure 1 in the main manuscript). From these we choose six states ( $|1\rangle \dots |6\rangle$ ) that are numbered in order of increasing energy, as depicted in figure SM2. Optical transitions take place between states of manifolds  $n$  and  $n - 1$  that differ by one e-h-pair, and we assume that two transitions ( $|6\rangle \rightarrow |5\rangle$  and  $|2\rangle \rightarrow |1\rangle$ ) are optically bright and resonant with the laser mode. A special role takes on the transition from the  $n = 1$  manifold to the ground state. In the experiment to which the model is applied, the ground-state exciton is strongly detuned from the cavity mode. In the configuration dynamics, the realization of the ground state is therefore strongly inhibited due to pumping, and the light-matter interaction is deter-

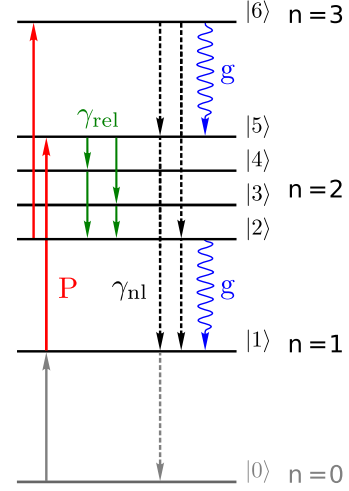


Figure SM 2. Schematic representation of the electronic QD level structure, corresponding to figure 1 (main manuscript) Light-matter coupling leads to recombination processes between the excitation manifolds with the light-matter coupling strength  $g$ . The arrows indicate the excitation, relaxation processes, and spontaneous emission into leaky modes taking place at a rate  $P$ ,  $\gamma_{rel}$  and  $\gamma_{nl}$ , respectively. Transitions between  $n = 1$  and  $n = 0$  are strongly off-resonant, thus the dynamics of the  $|0\rangle$  state is effectively described by  $|1\rangle$ , see text.

mined by the interplay of many-particle transitions between higher manifolds with  $n > 0$ . Therefore, the  $n = 0$  state is not included in the calculations.

The Hilbert space of the multi-QD and cavity-photon system is spanned by the product states  $|i_1\rangle \dots |i_{N_{QD}}\rangle |N\rangle$ , where  $|N\rangle$  defines the  $N$ -photon Fock state of the cavity mode. Considering the QDs and the photon mode as an open quantum system, one can describe the dynamics of the system density operator by the von Neumann-Lindblad (vNL) equation

$$\frac{\partial}{\partial t} \rho = -i[H_{JC}, \rho] + \mathcal{L}\rho. \quad (1)$$

The coherent dynamics is represented by the commutator with the Jaynes-Cummings (JC) Hamiltonian

$$H_{JC} = g \sum_{\alpha,i} \left[ b^\dagger D_{\alpha,i}^l + b (D_{\alpha,i}^l)^\dagger \right], \quad (2)$$

describing the non-perturbative light-matter interaction between the QD-interband transitions and the quantized field of the microcavity mode. Here, the operator

$$D_{\alpha,i}^l = \sum_j |\alpha, j\rangle \langle \alpha, i| \quad (3)$$

expresses all dipole-allowed transitions of QD  $\alpha$  between many-particle state  $|i_\alpha\rangle$  and  $|j_\alpha\rangle$  that are resonant with the laser mode, i.e.  $|6\rangle \rightarrow |5\rangle$  and  $|2\rangle \rightarrow |1\rangle$ .  $b^\dagger$  and  $b$  are the bosonic creation and annihilation operators for



photons in the laser mode, and  $g$  is the light-matter coupling strength for the respective electronic states and the cavity mode.

QDs are embedded systems, and their dynamics is strongly influenced by the coupling between localized QD states and the (quasi-) continuum of delocalized states and photon modes. While the former facilitates efficient carrier scattering into and within the QD via carrier-Coulomb and carrier-phonon interaction, the coupling to the latter leads to carrier recombination due to spontaneous emission. The incoherent, dissipative evolution results from the system-bath interaction, which leads to the sum of Lindblad operators

$$\mathcal{L}\rho = \sum_X \frac{\gamma_X}{2} [2X\rho X^\dagger - X^\dagger X\rho - \rho X^\dagger X]. \quad (4)$$

The operator  $X$  describes a reservoir-assisted transition in the system. The relevant information about the bath and its interaction with the system is contained in the transition rate  $\gamma_X$ . In the system we consider,  $X$  can be either a transition operator  $|i_\alpha\rangle\langle j_\alpha|$  between two QD many-particle states, or a photonic annihilation operator  $b$ . The first case corresponds to a change from many-particle state  $|j_\alpha\rangle$  to  $|i_\alpha\rangle$ , including pump excitation, spontaneous recombination into non-lasing modes and relaxation processes at rates  $P$ ,  $\gamma_{\text{nl}}$  and  $\gamma_{\text{rel}}$ , respectively. All occurring incoherent processes are schematically depicted in figure SM2. In the second case the photon subsystem undergoes a lowering of the photon number due to cavity losses at a rate  $\kappa$ .

The von Neumann-Lindblad equation (1) is solved numerically until the steady-state solution is reached. Then various steady-state expectation values, such as the level populations and the photon statistics can be obtained. For the calculations shown in the main text, a light matter coupling strength of  $g = 0.11/\text{ps}$  is used, corresponding to a vacuum rabi splitting of  $140\mu\text{eV}$ . For the intraband relaxation rates  $\gamma_{\text{rel}}$  we use  $0.5/\text{ps}$ . Radiative losses into non-lasing modes are strongly suppressed in photonic crystal cavity devices, and we consider  $\gamma_{\text{nl}} = 0.01/\text{ps}$ . The cavity decay rate of  $\kappa = 0.16/\text{ps}$  corresponds to a cavity-Q of 12000 in the spectral range of the InGaAs QD emission.

To calculate the pump-rate dependent spontaneous-emission coupling factor

$$\beta(P) = \frac{\Gamma(P)}{\Gamma(P) + \Gamma_{\text{nl}}(P)} \quad (5)$$

that is described by the ratio of the spontaneous emission into the lasing mode and the total spontaneous emission, at a given pump rate  $P$  we consider the equation of motion for the cavity mean photon number

$$\frac{d}{dt} \langle b^\dagger b \rangle = -\kappa \langle b^\dagger b \rangle + \Gamma + \Gamma_{\text{stim}}. \quad (6)$$

It is determined by the balance between cavity losses in the first term and photon emission. The second term constitutes the total spontaneous emission into the laser mode

$$\Gamma = \Gamma_{\text{spont}} + \Gamma_{\text{sr}}. \quad (7)$$

Here  $\Gamma_{\text{spont}}$  is the usual contribution from independent emitters to the spontaneous emission, and  $\Gamma_{\text{sr}}$  reflects the enhancement or suppression of spontaneous emission due to QD-QD correlations. The third term in Eq. (6) represents the contribution due to stimulated emission and absorption.

In the steady state we obtain

$$\Gamma_{\text{spont}} = \sum_{\alpha=1}^{N_{\text{QD}}} \sum_i R_i \langle (D_{\alpha,i}^l)^\dagger D_{\alpha,i}^l \rangle \quad (8)$$

and

$$\Gamma_{\text{sr}} = \sum_{\alpha \neq \beta}^{N_{\text{QD}}} \sum_{i,j} R_i \langle D_{\alpha,i}^l (D_{\beta,j}^l)^\dagger \rangle. \quad (9)$$

For more details we refer to Ref. [14]. The quantity  $R_i$  is the spontaneous emission rate for recombination of the many-particle state  $|i_\alpha\rangle$

$$R_i = \frac{4g^2}{\kappa + \gamma_i^{\text{tot}}}, \quad (10)$$

which resembles the form known from rate equations, where  $\gamma_i^{\text{tot}}$  is the total dephasing of the many-particle transition with the initial state  $|i_\alpha\rangle$ . Similarly, an expression for the emission into non-lasing modes can be found

$$\Gamma_{\text{nl}} = \gamma_{\text{nl}} \sum_{\alpha=1}^{N_{\text{QD}}} \sum_i \langle (D_{\alpha,i}^{\text{nl}})^\dagger D_{\alpha,i}^{\text{nl}} \rangle. \quad (11)$$

In this expression  $D_{\alpha,i}^{\text{nl}}$  describes all dipole-allowed transitions of QD  $\alpha$  that are detuned from the laser mode. Eqns. (5) - (11) are explicitly evaluated to obtain the pump-power dependent  $\beta(P)$ -factor introduced in the main text. All averages are taken with respect to the steady state density matrix.

---

\* [jonathan.finley@wsi.tum.de](mailto:jonathan.finley@wsi.tum.de)

† [michael.kaniber@wsi.tum.de](mailto:michael.kaniber@wsi.tum.de)

- [1] A. Kress, F. Hofbauer, N. Reinelt, M. Kaniber, M. Bichler, D. Schuh, G. Boehm, and J. J. Finley, Proc. SPIE **6182**, 114 (2005).
- [2] T. Yoshie, A. Scherer, J. Hendrickson, G. Khitrova, H. Gibbs, G. Rupper, C. Ell, O. Shchekin, and D. Deppe, Nature **432**, 200 (2004).

- [3] T. Asano, B.-S. Song, Y. Akahane, and S. Noda, Selected Topics in Quantum Electronics, *IEEE Journal of* **12**, 1123 (2006).
- [4] R. H. Brown and R. Twiss, *Journal of Astrophysics and Astronomy* **15**, 13 (1994).
- [5] M. Nomura, S. Iwamoto, T. Nakaoka, S. Ishida, and Y. Arakawa, *Applied physics letters* **88**, 141108 (2006).
- [6] M. Kaniber, A. Neumann, A. Laucht, M. Huck, M. Bichler, M. Amann, and J. Finley, *New Journal of Physics* **11**, 013031 (2009).
- [7] P. Michler, A. Kiraz, C. Becher, W. Schoenfeld, P. Petroff, L. Zhang, E. Hu, and A. Imamoglu, *Science* **290**, 2282 (2000).
- [8] C. Santori, M. Pelton, G. Solomon, Y. Dale, and Y. Yamamoto, *Physical Review Letters* **86**, 1502 (2001).
- [9] K. Hennessy, A. Badolato, M. Winger, D. Gerace, M. Atatüre, S. Gulde, S. Fält, E. L. Hu, and A. Imamoglu, *Nature* **445**, 896 (2007).
- [10] D. Press, S. Götzinger, S. Reitzenstein, C. Hofmann, A. Löffler, M. Kamp, A. Forchel, and Y. Yamamoto, *Physical Review Letters* **98**, 117402 (2007).
- [11] M. Kaniber, A. Laucht, A. Neumann, J. Villas-Bôas, M. Bichler, M.-C. Amann, and J. Finley, *Physical Review B* **77**, 161303 (2008).
- [12] U. Hohenester, A. Laucht, M. Kaniber, N. Hauke, A. Neumann, A. Mohtashami, M. Seliger, M. Bichler, and J. J. Finley, *Physical Review B* **80**, 201311 (2009).
- [13] A. Laucht, M. Kaniber, A. Mohtashami, N. Hauke, M. Bichler, and J. Finley, *Physical Review B* **81**, 241302 (2010).
- [14] H. Leymann, A. Foerster, F. Jahnke, J. Wiersig, and C. Gies, *Physical Review Applied* **4**, 044018 (2015).